Photopolymerization of Imprinted Polymer with Dummy Template for the Recognition of Hydroquinone in Aqueous Medium

Norlin Suhaiza Musali[1], Norlaili Abu Bakar[1*], Nurulsaidah Abdul Rahim[1], Wan Rusmawati Wan Mahamod[1], Norhayati Hashim[1,2], Sharifah Norain Mohd Sharif[1], Siti Kamilah Che Soh[3], and Alizar Ulianas[4]

[1]*Department of Chemistry, Faculty of Science and Mathematics, Universiti Pendidikan Sultan Idris, Tanjong Malim 35900, Malaysia*

[2]*Nanotechnology Research Centre, Faculty of Science and Mathematics, Universiti Pendidikan Sultan Idris, Tanjong Malim 35900, Malaysia*

[3]*Faculty of Science and Marine Environmental, Universiti Malaysia Terengganu, Kuala Nerus 21030, Malaysia*

[4]*Department of Chemistry, Faculty of Mathematics and Natural Sciences, Universitas Negeri Padang, Jl. Prof. Dr. Hamka, Padang 25173, Indonesia*

Corresponding author:

email: norlaili@fsmt.upsi.edu.my

Received: October 26, 2023
Accepted: June 4, 2024

DOI: 10.22146/ijc.90096

Abstract: *This study' purposes are to synthesize molecularly imprinted polymer (MIP) with hydroxyethyl methacrylate (HEMA) and triethylene glycol dimethacrylate (TEGDMA) using* p*-xylene under ultraviolet curing at 405 nm for the recognition of hydroquinone (HQ) in aqueous medium. The template was extracted from the polymer with a mixture of methanol and acetic acid (9:1) by volume (v/v). The Fourier transform infrared (FTIR) spectrum of MIP (after wash) showed the absence of peak at the range of 840–860 cm^{-1}, which represented the stretching outside the aromatic plane C–H at the para position (*p*-xylene). Field emission scanning electron microscope (FESEM) micrograph showed that the MIP had cavities compared to non-imprinted polymer (NIP). The MIP (MIP-Pxy) with ratio (monomer:crosslinker) 0.25 and 1.00% template gave the highest uptake of hydroquinone (HQ) in aqueous solution, which implied more specific recognition (highest K_D value). The rebinding of HQ onto MIP-Pxy was best described by both isotherm (Langmuir and Freundlich) and kinetic model (pseudo-first and -second). The MIP was successfully synthesized using* p*-xylene, able to recognize HQ and was very selective to* p*-CP. Implication of the study, the synthesized MIP can be used for recognition and sensing materials for HQ and any similar molecules.*

Keywords: *imprinting factor;* p*-xylene; phenolic compound; electron donor-acceptor; adsorbate*

Accepted

■ INTRODUCTION

Hydroquinone (HQ) is an aromatic compound with white to grey crystal appearance. There are three isomers of dihydroxybenzene, which are resorcinol (RC), catechol (CC) and HQ [1]. HQ is a compound of di-substituted phenol (1,4-dihydroxybenzene), it is a very common chemical in the environment due to being widely used in various fields such as in coloring, cosmetics, photo-stabilizers, pharmaceuticals, oil refineries, plasticizers, pesticides, and textiles [1-3]. In cosmetics, HQ is widely used as a whitening agent which prevents the hyperpigmentation of skin [4]. The standard amount of allowed HQ by the United States Food & Drug Administration (USFDA) is 2–5% in skin care products [5]. In phenol wastewaters, the presence of HQ and *p*-benzoquinone at early stages of phenol oxidation increases the water toxicity, which implies that these compounds are more toxic and less degradable than the

original pollutant [6].

Uncontrolled HQ exposure causes skin sensitization, irritation, hyperpigmentation, and nail discoloration [4]. Aside from its skin effects, HQ has been discovered to expose consumers to acute oral toxicity and can induce disorders such as thyroid dysfunction, leukemia, and liver damage [7]. Monitoring the usage of HQ in consumer products and controlling the exposure of this compound needs to be taken seriously by industrial, consumer and government to prevent long-term effects. There are various scientific methods used to detect and remove this substance from water, food, and cosmetics, such as cultivation [8], chromatographic [9], spectrometric [10], and adsorption [11], respectively. Various materials can be used for the removal, detection, and determination of HQ, such as plants [8], *Phragmites australis* activated carbon [12], electrode material [13], biosensor [14], chemical sensors [15], and molecularly imprinted polymers (MIP) [16]. In all methods involving removal, detection, and determination of HQ, specific recognition of the target molecules or compound plays an important role in giving higher removal, good detection, and accurate determination results.

MIP is one of the materials that give specific recognition against target molecules. MIPs have been widely used for various applications, including separation, solid-phase extraction, and sensors, because of their various benefits, including precise identification, chemical stability, and relatively inexpensive and simple manufacture [17]. MIP have gained attention due to their unique properties that can recognize more specific molecules [18]. Molecular imprinting is a promising method for producing polymers with pre-set selectivity, specificity, and high affinity for a target molecule. It refers to the assembly of polymerizable functional monomers around a template molecule [19]. Molecularly imprinted polymers have the ability to specifically distinguish and separate a specific molecule from other molecules with similar structures [20]. It is proficient in imitating the selective binding of target molecules. Its usage as a catalyst, sensor, drug delivery component, etc., has made it well-known for its numerous uses in various scientific domains [21].

Functional monomers such as hydroxyethyl methacrylate (HEMA) are the most frequently used because of their excellent properties as a hydrogen bond donor and acceptor [18]. The presence of triethylene glycol dimethacrylate (TEGDMA) in the polymer network enhances the hydrophilic properties of imprinted materials [22], which eases the template removal process during the washing process and analyte rebinding. The template is the target molecule or any molecule similar to it. The use of a template that resembles the target molecule (dummy template) in a MIP can prevent leakage of the template (target molecule) into the sample extract and interfere with the determination of the concentration of the analyte (target molecule) [23].

Generally, MIPs are prepared by free radical polymerization, which can be done by various types of polymerizations such as bulk, emulsion, solution and suspension. Thermal polymerization requires a longer reaction time with the presence of an initiator and uses many organic solvents in previous studies. Nowadays, radiation polymerization technology such as UV, gamma-ray, electron beam, and microwave radiation have been used in MIP synthesis [24], which can shorten the reaction time and sometimes without the presence of an initiator. Aside from reaction time, radiation technology reduces the usage of organic solvents which lower the environmental pollution and safety risks [25].

There is not much reported elsewhere about the synthesis of MIP for HQ recognition. During the synthesis of thermal polymerization, nitrogen gas flows continuously or for several hours if HQ is used as a template [26]. However, using a dummy template, namely *p*-xylene does not require N_2 gas to flow continuously. Hence, in this study, a dummy template (*p*-xylene) imprinted polymer was prepared via photopolymerization for the recognition system of HQ in an aqueous solution.

■ EXPERIMENTAL SECTION

Materials

All chemicals, namely HQ, HEMA, TEGDMA, camphorquinone, ethyl 4-(dimethylamino)benzoate

Accepted

(EDMAB) and *p*-xylene used in this study were purchased from Sigma Aldrich. Acetic acid (CH_3COOH) and methanol (CH_3OH) were purchased from Systerm. All solutions were prepared by using distilled water. The buffer solutions were prepared in the range of pH 4–9 using acetic acid, sodium acetate (CH_3COONa), dipotassium hydrogen phosphate (K_2HPO_4), potassium dihydrogen phosphate (KH_2PO_4), trizma base, and HCl. All monomers were first purified before use.

Instrumentation

The instruments used in this study are Thermo Nicolet Nexus Spectrophotometer FTIR for analysis of functional groups on MIP and NIP. The Hitachi 8U 8020 UHR FESEM analyzed the surface morphology of MIP and NIP, and a Perkin Elmer Ultraviolet spectrophotometer was used to follow the recognition study of MIP against HQ in an aqueous solution. All instruments used are in Universiti Pendidikan Sultan Idris.

Procedure

Synthesis and characterization of p*-xylene imprinted polymer*

A molecularly imprinted polymer solution was prepared by mixing together HEMA (monomer), TEGDMA (crosslinker) and 0.1 g camphorquinone (initiator), giving a total mixture mass of 10 g. The monomer/crosslinker was varied in a weight ratio (wt/wt) of 0.25, 1.00, and 4.00. Three different template (*p*-xylene) percentages (0.5, 1.0 and 3.0%) were added to the total mass of the mixture. The same composition was used to prepare NIP without the need for templates. The *p*-xylene acted as a dummy template and it is important to allow the formation of cavities in the polymer that are very similar to the target compound (HQ) as they have the similar molecular structure. These solutions (250 µL/mould) were poured into several mould (1 × 1 cm) and underwent photopolymerization with ultraviolet at 405 nm for 30 min. To remove *p*-xylene, the polymer strips were washed with a solvent mixture (methanol:acetic acid) in a 9:1 (v/v) ratio [27] for 6 h using the Soxhlet apparatus. Using a mixture of methanol and acetic acid to remove template molecules from molecularly imprinted polymers gave a high-efficiency percentage of 90.75% [28]. The polymer strips will then be dried in an oven and kept in a sample bottle before being used for further characterization and experiments.

The MIP strip was characterized with FTIR to ensure the elimination of the template (*p*-xylene) after the washing stage. Aside from that, this analysis provides confirmations of functional groups and covalent bonding information that were present in the MIP strip. The detection range was between 650–4000 cm^{-1} at room temperature using the ATR method by FTIR instrument. The surface morphology of the MIP strip was examined using FESEM. The presence of cavities on the surface of the MIP proves the successful extraction of the dummy template (*p*-xylene).

Recognition study of HQ in aqueous medium

The recognition study was done by immersing the imprinted polymer (MIP-Pxy) strip with different ratios of monomer/crosslinker into 10 mL of 50 mg L^{-1} HQ for 20 min separately. After that, the strip was removed, and the absorbance intensity of the remaining solution was measured with an ultraviolet spectrophotometer at 289 nm. The absorbance intensity of HQ solution before immersing the strip of MIP was also measured using the same method. Experiments were repeated 3 times to ensure a good data value.

The recognition study proceeded with the adsorption of HQ onto MIP-Pxy with different loading percentages of template (*p*-xylene). The best ratio of MIP-Pxy with different percentages of *p*-xylene was immersed in 10 mL of 50 mg L^{-1} HQ for 20 min. After 20 min, the remaining concentration was analyzed for absorbance intensity at 289 nm. MIP-Pxy with the best ratio (monomer/crosslinker) and percentage template were used in pH, kinetic, isotherm and selectivity studies. For the pH study, the MIP-Pxy strips were immersed in 50 mg L^{-1} HQ solution with different pH (4–9) for 20 min, separately. The MIP-Pxy was also immersed in HQ solution with different initial concentrations (30, 50, and 100 mg L^{-1}) at various time intervals (2, 4, 6, 8, 10, 20, 30, and 40 min) separately to determine the steady-state equilibrium time and kinetics behavior. In the isotherm study, the strips were

Accepted

immersed in various concentrations of HQ (2–100 mg L^{-1}) for 20 min. The selectivity study was done with a similar molecule structure of HQ, namely *p*-nitrophenol (*p*-NP) *p*-chlorophenol (*p*-CP) and *p*-methylphenol (*p*-MP). The MIP-Pxy was immersed into 10 mL of 50 mg L^{-1} similar molecule structure solution for 20 min separately. The absorbance intensity of all experiments (pH, kinetic, isotherm and selectivity study) was measured with an ultraviolet spectrophotometer at 289 nm.

Equilibrium time was the time taken by the HQ molecule to be adsorbed on the surface and into the cavities that exist in the MIP. From the adsorption kinetic study performed, the imprinting factor (α) and the distribution coefficient (K_D) can be determined. The K_D can determine the specific adsorption performed by molecular printed polymers compared to non-imprinted polymers. It can be determined from the formula in Eq. (1) [29].

$$K_D = \frac{C_p}{C_s} \quad (1)$$

K_D is the equilibrium constant of the binding site. C_s is the analyte concentration at equilibrium, and C_p is the amount of analyte adsorbed per gram of MIP. High imprinting factor values indicate good imprinting and can provide good identification properties of the target molecule. The imprinting factor (α) in turn, distinguishes the adsorption of MIP and NIP. It can be determined from the formula in Eq. (2) [29].

$$\alpha = \frac{K_D(\text{MIP})}{K_D(\text{NIP})} \quad (2)$$

According to Hasanah et al. [30], the imprinting factor describes how effectively MIP owns the quality of imprinted sites. The factor was calculated by dividing the MIP distribution coefficient by the number of NIPs. A higher value of K_D MIP than K_D NIP indicates a good imprinting factor; hence, a K_D value greater than one indicates a good imprinting factor.

The Lagergren pseudo-first-order and pseudo-second-order kinetic models were used to evaluate the adsorption kinetics of HQ onto MIP and NIP. The pseudo-first-order kinetic model describes the link between the adsorbent sorption site occupancy rate and the number of vacant sites. It is defined as follows using the Lagergren pseudo-first-order Eq. (3):

$$\ln(q_e - q_t) = \ln q_e - k_1 t \quad (3)$$

where q_e and q_t are the quantity of HQ adsorbed at equilibrium and time t (min), and k_1 is the adsorption rate constant (min^{-1}). The rate constant k_1 was calculated using a linear plot of $\ln(q_e-q_t)$ over time [31]. The pseudo-second-order kinetic model describes the time dependence of the adsorbent's adsorption capacity and may be calculated using Eq. (4). It is written as follows.

$$\frac{t}{q_t} = \frac{1}{k_2 q_e^2} + \frac{t}{q_e} \quad (4)$$

The pseudo-second-order rate constant (g mg^{-1} min^{-1}) is denoted by k_2. The slope and intercept of the linear plot of t/q_t against time are used to calculate q_e and k_2 [31].

The Langmuir isotherm (Eq. (5)) and Freundlich isotherm (Eq. (6)) are the two most often utilized linearized adsorption isotherms. The Langmuir isotherm model assumed that there were a finite number of active sites that were uniformly distributed across the adsorbent's surface. There is no interaction between adsorbed molecules, and these active sites have the same affinity for a monomolecular layer's adsorption [32]. The Freundlich isotherm model, which is not limited to the development of a monolayer, applies to adsorption on heterogeneous surfaces with interaction between the adsorbed molecules. This model assumes that as the adsorbate concentration increases, so does the concentration of adsorbate on the adsorbent surface and that the adsorption energy drops exponentially upon completion of the process [33]:

$$\frac{C_e}{q_e} = \frac{1}{q_m K_L} + \frac{1}{q_m} C_e \quad (5)$$

$$\log q_e = \log K_F + \frac{1}{n} \log C_e \quad (6)$$

where q_m is the maximum adsorption capacity, K_L is the Langmuir constant, K_F is the Freundlich constant, 1/n is the sorption intensity parameter related to material heterogeneity, and n is an empirical parameter with values ranging from 1 to 10 indicating favorable adsorption [34]. The n value shows the degree of nonlinearity between solution concentration and

Accepted

adsorption as follows: if n = 1, adsorption is linear; if n < 1 is a chemical process; and if n > 1 is a physical process [35].

■ RESULTS AND DISCUSSION

Synthesis and Characterization of *p*-Xylene Imprinted Polymer

Fig. 1(a) shows FTIR spectrum of MIP-Pxy before and after the washing stage, NIP and template (*p*-xylene). The presence of *p*-xylene in MIP before wash can be observed in the region of 840–860 cm^{-1}, which corresponded to stretching beyond the plane of the aromatic C–H in the para position and at 1451 cm^{-1} due to the vibration of the aromatic compound's benzene ring backbone C=C [36]. These peaks vanished after the washing and drying stage. The presence of C=O groups in HEMA and TEGDMA was linked to the appearance of a peak at 1719 cm^{-1} [37]. The stretching vibrations of aliphatic C–H from *p*-xylene, HEMA, and TEGDMA were ascribed to the peaks at 2872–2951 cm^{-1}.

In the synthesis of MIP, monomer units consisted of functional groups evenly distributed throughout the template material via non-covalent or covalent interactions. The degree of cross-linking in polymerization assists in the retention of functional groups in specified places by the polymer networks. Because of its ability to form hydrogen bonds between the molecules of templates and hydroxyl groups, HEMA is the most often employed monomer for this modification [38]. When *p*-xylene is involved in molecular imprinting, an interaction known as the "π-π interaction" occurs with the functional group [39]. In a study that created MIP sensor to detect 4-NP and HQ, it was discovered that π-π interaction also takes place between the functional monomers and these aromatic rings [27]. Therefore, it was anticipated that interactions in this study would take place at the binding sites through π-π interactions. The dipole of the carboxylic group in methacrylic acid will interact with the active ring

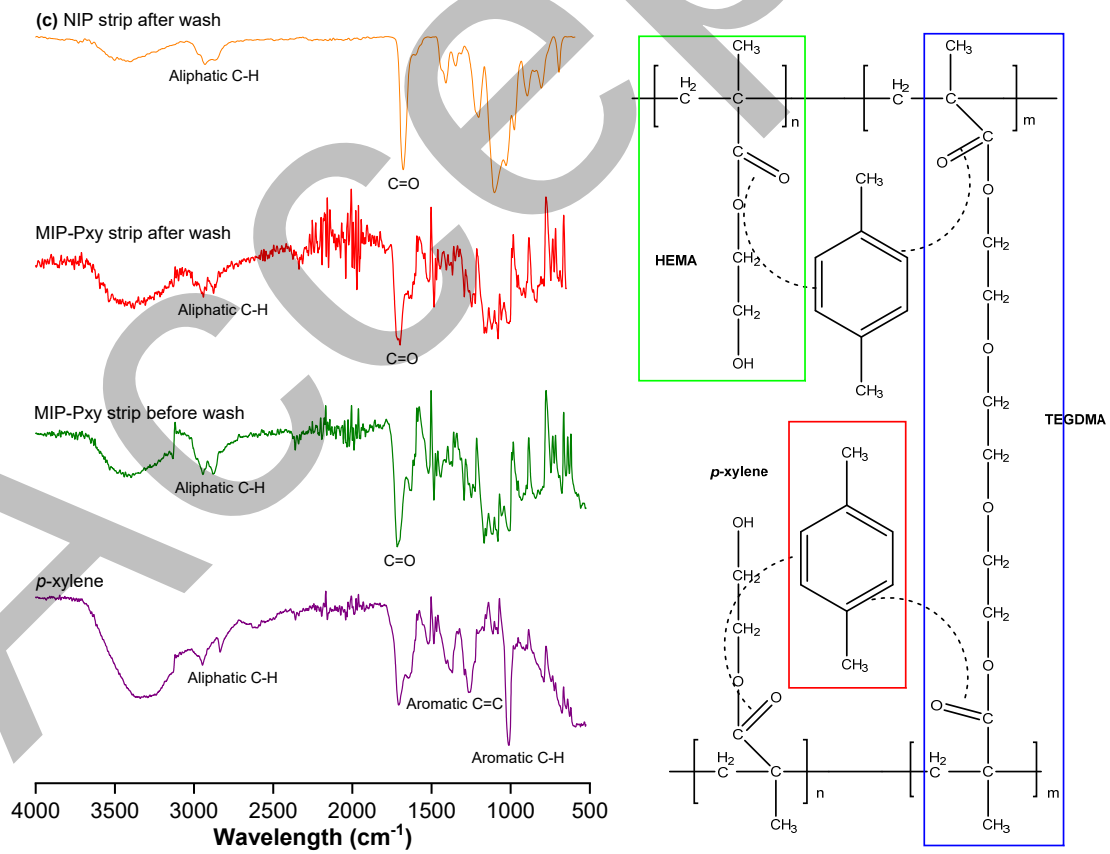

Fig 1. The (a) FTIR spectrum and (b) interaction of monomer, crosslinker and *p*-xylene in MIP synthesis [the ratio composition of MIP and NIP is 0.25 (monomer:crosslinker) and 1% template]

Accepted

of benzene in *p*-xylene (Fig. 1(b)). The π-π interaction of the monomers, crosslinkers and the template occurred via a covalent bond [40].

Fig. 2 shows the micrograph images of synthesized products in the form of strips which were MIP-Pxy before and after the washing stage, and NIP using FESEM. The presence of cavities (red arrow in Fig. 2(b)) on MIP-Pxy after the washing stage is more obvious compare to Fig. 2(a) (before the washing stage) due to the removal of the template with methanol and acetic acid, while no cavities present on the surface of NIP (Fig. 2(c)). This was consistent with the findings by Limthin et al. [41], which explained that the template removal led to the enhanced presence of cavities in the polymeric matrix thus making it easier for molecular interaction to take place. According to Bakhtiar et al. [42], the absence of a cavity in NIP was due to the absence of a template during the synthesis. Hence, no effective confined shrinkage occurred during the polymerization process.

Recognition Study of MIP-Pxy against HQ in Aqueous Medium

The effect of monomer/crosslinker ratio and template percentage

The monomer-cross linker optimization of MIP-Pxy was done to determine the best rebinding of HQ onto MIP. It was found that the highest uptake of HQ occurred to MIP-Pxy with a monomer-crosslinker ratio of 0.25, followed by 1 and 4 (Fig. 3). It was strongly believed that higher crosslinker content gives better rebinding of HQ onto MIP-Px. This finding is comparable to that of Retnaningtyas et al. [43], who discovered that the highest volume of cross-linker improved the cavity's ability to recognize template molecules as well as the stability of the polymer framework and the similarity of cavity structures to template molecules. The ratio of the functional monomer to the template molecule, the amount of cross-linker, and the reaction solvent all have effects on the polymer's specific recognition ability to identify the target molecule during MIP development [44]. Excessive functional monomer or cross-linker could lead the imprinted layer to be excessively thick, hence lowering the luminous efficiency of the sensor. However, if inadequate monomer and cross-linker are utilized, the imprinting process fails, resulting in a decrease in sensitivity.

A few possible interactions are used to explain the bonding that happens between the functional groups of monomers on the surface of MIP with HQ (Fig. 4).

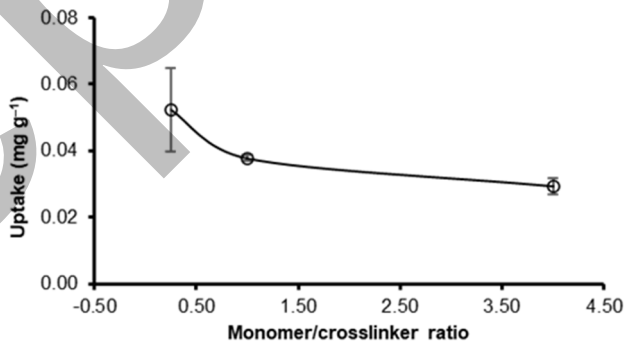

Fig 3. The effect of monomer/crosslinker ratio against rebinding uptake of HQ onto MIP-Pxy in aqueous solution

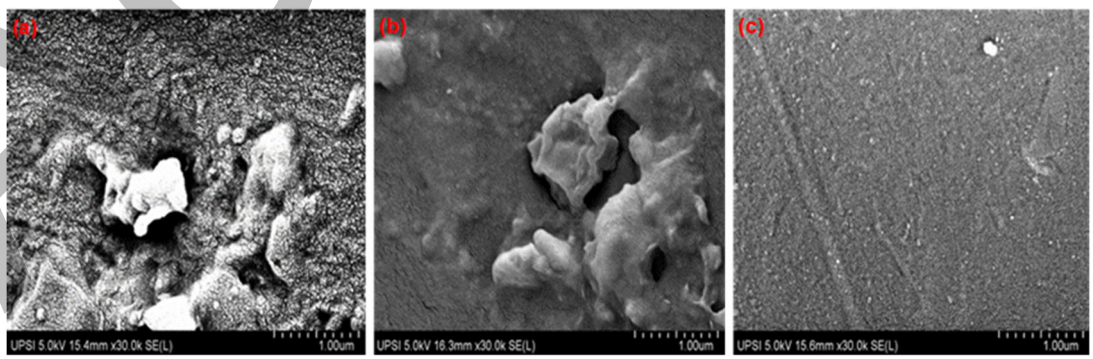

Fig 2. FESEM micrograph of (a) MIP-Pxy before, (b) MIP-Pxy after, and (c) NIP after wash with a mixture of methanol/acid acetic (9/1) by volume (v/v) [magnification scale is 30.0k and the ratio composition of MIP and NIP is 0.25 (monomer:crosslinker) and 1% template]

Accepted

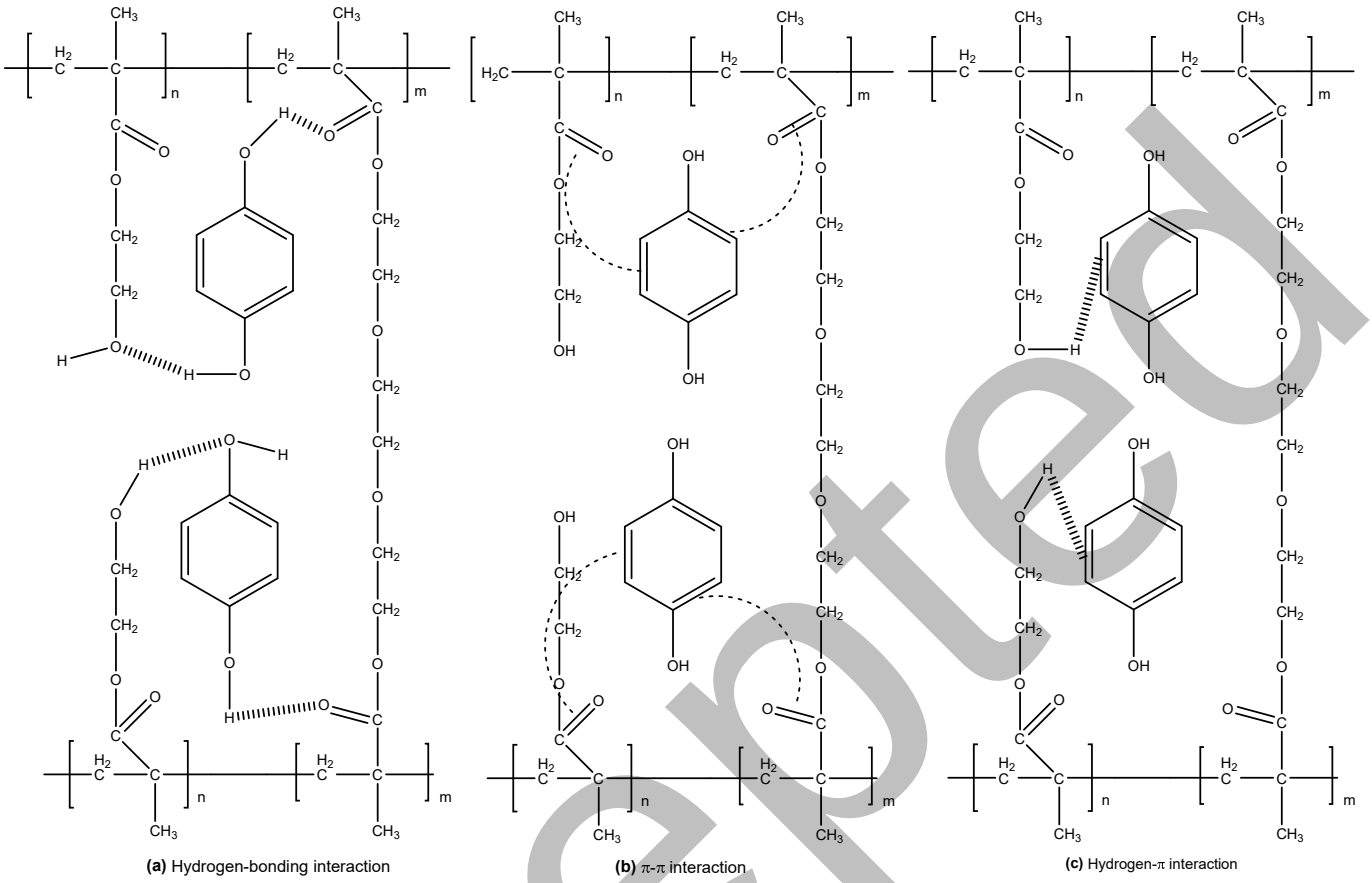

Fig 4. The possible interaction of HQ, crosslinker (TEGDMA) and monomers (HEMA) on the surface of MIP

Among the possible interactions that occur is hydrogen bonding. The hydroxyl group from HEMA will interact with oxygen atom from the hydroxyl group of HQ (Fig. 4(a)). Similar interactions are also obtained in the study made by Masumoto et al. [45], which has synthesized MIP using methacrylamide and 4-vinylpyridine as functional monomers while arbutin and rutin as the template molecules. They stated that hydrogen bonding interactions between methyl methacrylate monomers and hydroxyl group(s) were applied in the recognition of their MIP as arbutin is a simple glycoside that has HQ as part of it. The hydrogen bond interaction also occurred between TEGDMA and the hydroxyl group of HQ. According to Comeau and Willet [46], TEGDMA has six oxygen atoms (ester and ether group) that act as hydrogen bond acceptors, which makes TEGDMA easily interact with hydrogen bond donors.

The second possible interaction in the recognition mechanism is polar-π interaction (Fig. 4(b)). Functional monomers (HEMA and TEGDMA) are polar monomers. The polar condition allows polar-π interaction to occur with the active benzene ring in the HQ. According to Rubahamya et al. [47], the most widely accepted mechanism for aromatic adsorption onto porous carbons is the π-π bonding idea. According to the π-π bonding theory, bonding develops between two p orbitals as a result of electron delocalization in the 2p orbitals around the benzene ring. This delocalization allows weak π bonds to form at the basal planes of the benzene rings that make up the porous carbon adsorbent's surface. The distribution of the π electron density is influenced by the surface functional groups of porous carbon, where electron-withdrawing groups form positive holes within the π electron system, lowering the adsorptive potential of the porous carbon. Electron-donating functional groups, on the other hand, increase the electron density in the π-electron system and thus the adsorptive potential of the porous carbon adsorbent.

Accepted

Fig. 4(c) shows the last possible interaction which is hydrogen-π interaction that occurs between π in active benzene ring of HQ and the –OH functional group of HEMA. This observation is consistent with the findings of Grissom et al. [48], who stated that hydrogen bonding can occur in any molecule with electron-rich areas, including aromatics. Computational studies have shown that hydrogen bonding between –OH groups and aromatic groups is followed by an electron density transfer from the acceptor of the hydrogen bond to the donor O–H bond's -antibonding orbital.

Fig. 5(a) shows the rebinding of HQ onto MIP-Pxy at different template percentages. The highest uptake occurred to MIP-Pxy with 1% of the template. According to Retnaningtyas et al. [43], the ratio of functional template monomers and the ratio of functional molecular cross-linking monomers were key elements to consider in the synthesis of MIPs. An increase in template concentration could have resulted in overpopulation near the MIP, as well as a scarcity of binding sites. This is the fundamental reason why MIPs have a low affinity and selectivity when exposed to high template concentrations. MIPs, on the other hand, demonstrate great affinity and selectivity at low template concentrations, where high-affinity sites dominate the MIP's binding properties [49].

The effect of pH on the rebinding of HQ in aqueous solution onto MIP-Pxy is shown in Fig. 5(b). It was found that the highest uptake of HQ is at pH 6. There was low uptake found after pH 6. The same result was obtained by Mohanadas et al. [49], who found that the optimum pH condition for HQ in aqueous medium is at pH 6. According to Loreto et al. [50], the presence of a buffer will result in a lower adsorption capacity. This is because diffusion within the pores becomes more difficult in the presence of strong interactions. The increased interaction with the surface (via the phosphate group of the phosphate buffer molecule), which reduces desorption from the surface and hence slows surface diffusion, also contributes to an increase in adsorption uptake in acidic media.

The Kinetic Study

The rebinding of HQ onto MIP-Pxy and NIP is shown in Fig. 6. It was noted that initially, the adsorption was fast within the first 5 min (region I) and then tended to secure a saturated value. After 10 min (region II), the adsorption becomes constant and continues to remain. The short time required to reach the binding equilibrium denoted that the adsorption process was fast. During the process, a molecular memory was introduced into the polymer matrix after extracting the template, in which cavities complementary to HQ molecules were present so that the polymer was able to remember and rejoin the template [51]. In NIP, the adsorption slightly occurred and increased drastically before 10 min and decreased which showed no adsorption occurred for NIP. This means that the elevated adsorption rate at the starting stage could be

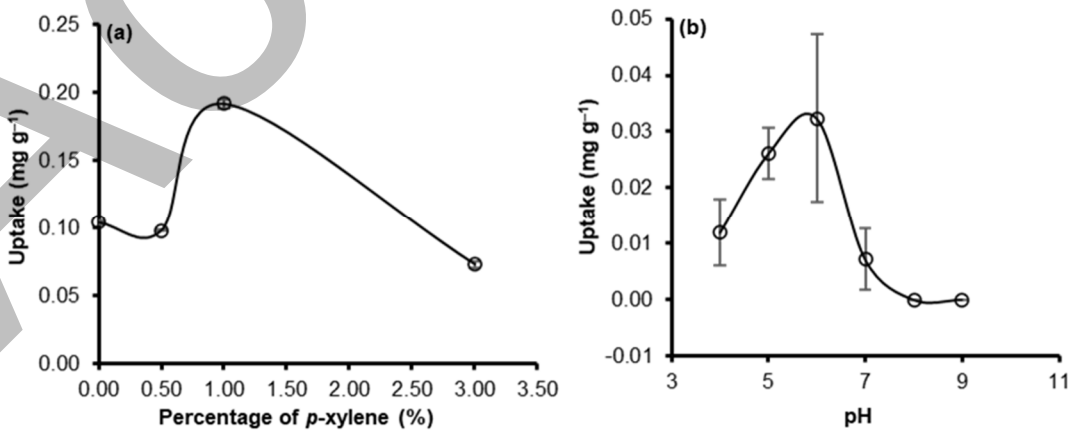

Fig 5. The effect of (a) template percentage and (b) pH on the rebinding of HQ onto MIP-Pxy in aqueous medium [the ratio composition of MIP and NIP is 0.25 (monomer:cross-linker) and 1% template]

Accepted

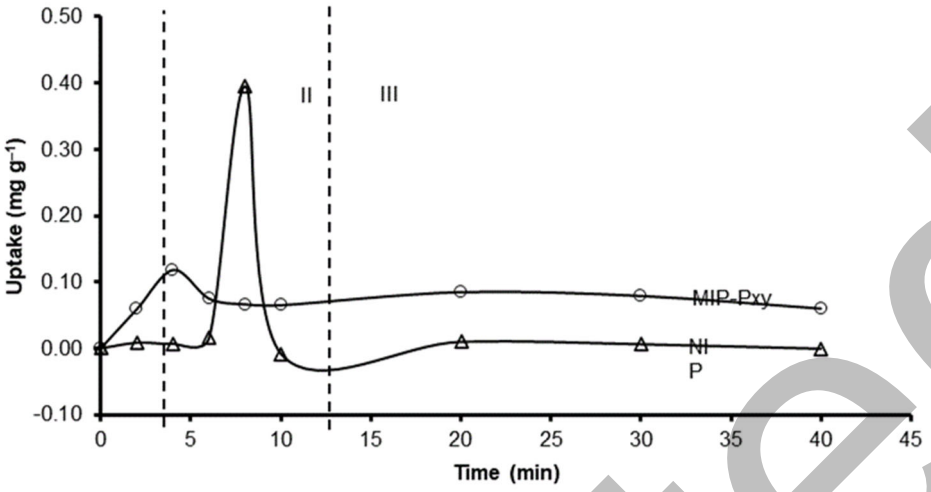

Fig 6. Equilibrium time for HQ adsorption on NIP and MIP-Pxy in aqueous solution. [HQ] = 50 mg L^{-1} [the ratio composition of MIP and NIP is 0.25 (monomer:cross-linker) and 1% template]

attributed to the existence of a significant fraction of unoccupied sites on the MIP-Pxy and NIP surfaces. The decreased rate may arise after 20 min due to the incremental occupation of these sites [52]. However, the adsorption of HQ on MIP-Pxy is higher than NIP because it was influenced by the presence of cavities that enhance the site of HQ recognition [53].

The kinetic model of Lagergen's pseudo-first-order and pseudo-second-order linear equations was used to examine the mechanism of HQ rebinding on MIP-Pxy. Fig. 7 shows the linear regression plots of pseudo-first and pseudo-second order, respectively, while Table 1 shows the derived kinetic parameters. Both kinetic model ($r^2 > 0.9$) best describes the adsorption mechanism of 30 and 50 mg L^{-1} HQ onto MIP-Pxy. Pseudo-first-order kinetic model shows the monolayer adsorption [54], and pseudo-second-order shows chemical adsorption, which involves sharing or exchanging electrons between

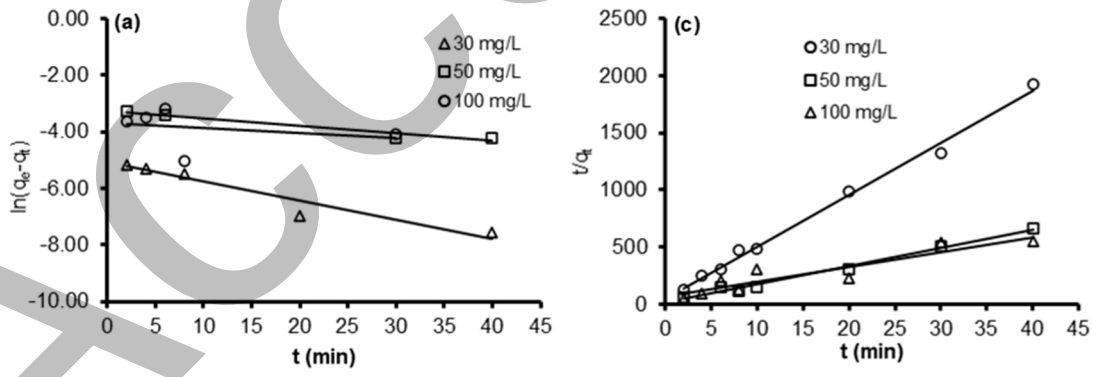

Fig 7. The (a) pseudo-first-order and (b) pseudo-second-order kinetics model of HQ rebinding onto MIP-Pxy at various initial concentrations [the ratio composition of MIP is 0.25 (monomer:cross-linker) and 1% template]

Table 1. The value of constant k at the different initial concentration

C_o (mg L^{-1})	$q_{e,exp}$	Pseudo-first-order			Pseudo-second-order		
	(mg g^{-1})	q_{e1} (mg g^{-1})	k_1 (min^{-1})	r^2	q_{e2} (mg g^{-1})	k_2 (min^{-1})	r^2
30	0.021	6.19×10^{-3}	0.068	0.925	0.022	40.780	0.994
50	0.075	0.039	0.027	0.959	0.062	24.340	0.989
100	0.072	0.025	0.017	0.077	0.077	2.580	0.852

Accepted

adsorbate and adsorbent [55]. Pseudo-second order was most reported as the best kinetic model to describe the adsorption or removal of analyte in aqueous solution [12,56-57].

The data in Fig. 8 demonstrate the influence of the initial concentration of HQ in the rebinding process on MIP-Pxy at 30, 50, and 100 mg L^{-1}. The result showed the highest and most stable rebinding occurred at the initial concentration of 50 mg L^{-1}. Table 2 showed that the value of K_D for MIP-Pxy for all concentrations was higher than NIP, which showed that MIP-Pxy gave specific recognition compared to NIP. However, the values obtained were less than 1. According to Hasanah et al. [30], $K_D > 1$ shows a good imprinting factor (α) value. The MIP-Pxy demonstrates the highest value of α at an analyte concentration of 50 mg L^{-1}, implying good α (K_D MIP > K_D NIP). Higher α value played a better key role in target recognition of specific binding sites on the MIP [29].

Isotherm and Selectivity Study of HQ, *p*-MP, *p*-NP and *p*-CP in Aqueous Medium

The rebinding of HQ onto MIP-Pxy is tested with Langmuir and Freundlich isotherm (Fig. 9). It was found that the rebinding of HQ onto MIP-Pxy was well-fitted with Freundlich and Langmuir isotherm with r^2 almost to 1. The experimental adsorption data indicate monolayer adsorption and a heterogeneous distribution of active sites on the MIP surface [58]. The Freundlich isotherm n value (Table 3) demonstrated the adsorption of HQ onto MIP-Pxy, which has strong physical adsorption. Values of n in the 1–10 range indicate good adsorption [35].

The selectivity of the MIP-Pxy in recognizing HQ is tested by comparing the adsorption of HQ with similar molecular structures (para-position) (Fig. 10). The selected molecules were *p*-CP, *p*-NP and *p*-MP. The K_D values for the adsorption indicate that the MIP-Pxy was more selectively recognized against *p*-CP (Table 4). The K_D value of *p*-CP was the highest compared to other

Table 2. The imprinting factor (α) and distribution coefficient (K_D) for MIP-Pxy and NIP at different concentrations of HQ

Concentration (mg L^{-1})	K_D		α
	MIP-Pxy	NIP	
30	6.80×10^{-4}	3.9×10^{-4}	1.76
50	1.45×10^{-3}	1.6×10^{-4}	8.91
100	7.80×10^{-4}	6.3×10^{-4}	1.22

Table 3. Langmuir and Freundlich parameters for the rebinding of HQ onto MIP-Pxy

Langmuir			Freundlich		
r^2	q_m (mg g^{-1})	K_L	r^2	n	K_F
0.946	0.016	0.377	0.992	4.031	0.006

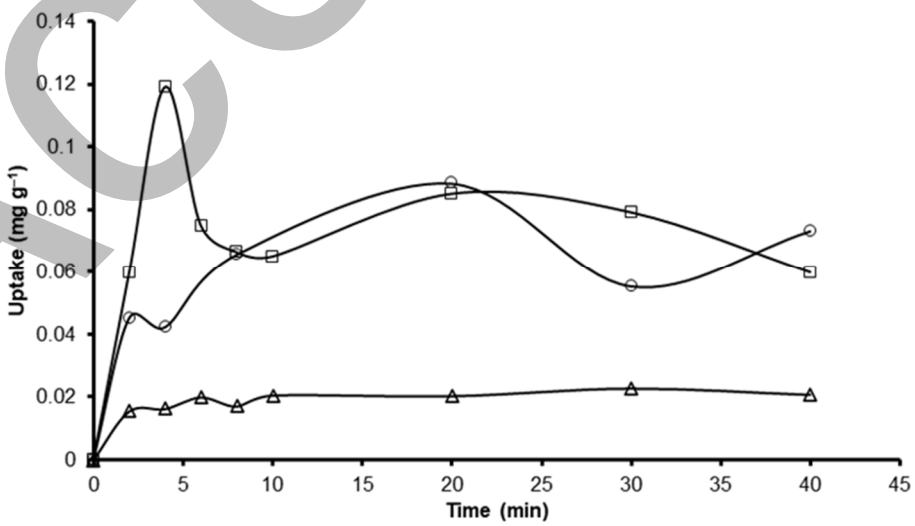

Fig 8. Effect of initial concentration of HQ in rebinding process onto MIP-Pxy at 30, 50, and 100 mg L^{-1} [the ratio composition of MIP is 0.25 (monomer:cross-linker) and 1% template]

Accepted

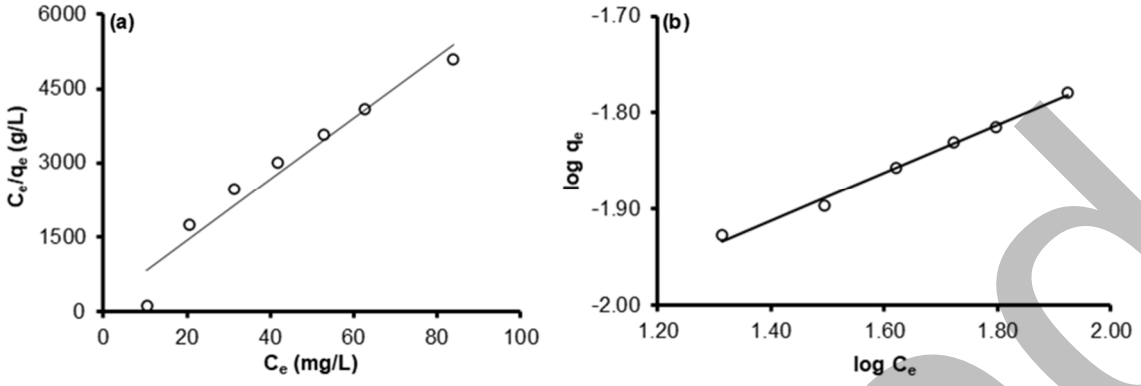

Fig 9. The (a) Langmuir and (b) Freundlich isotherm plot for rebinding of HQ onto MIP-Pxy in aqueous solution [the ratio composition of MIP is 0.25 (monomer: cross-linker) and 1% template]

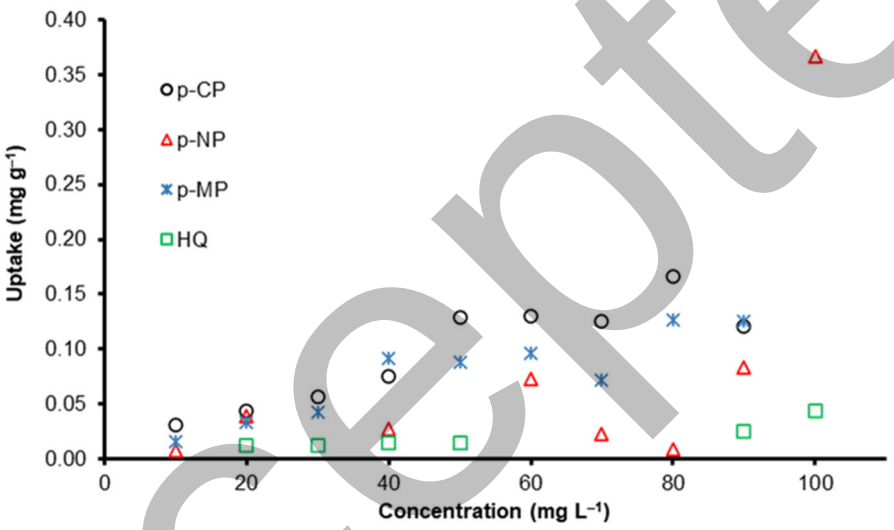

Fig 10. Selective recognition of HQ, *p*-CP, *p*-NP and *p*-MP onto MIP-Pxy in aqueous solution

Table 4. Distribution coefficient K_D for the selectivity of the phenolic compound onto MIP-Pxy

Phenolic compound	K_D
HQ	3.341×10^{-4}
p-CP	1.763×10^{-3}
p-NP	1.761×10^{-3}
p-MP	1.375×10^{-3}

molecules. According to Hou et al. [59], a higher value of K_D, a higher adsorption capacity. HQ exhibited a lower K_D value than others. However, all compounds have a similar structure, the specific molecular size and stereochemical structure differ, causing the variance in K_D values [60]. The presence of chlorine substituents (donating electron characteristics) in *p*-CP results in an improved electron-donor-acceptor (EDA) interaction between adsorbent and adsorbate [61].

■ CONCLUSION

The MIP-Pxy was successfully synthesized by photopolymerization for the recognition system of HQ in the aqueous medium. The synthesized MIP has the capability to recognize HQ as compared to non-imprinted polymers via π–π, polar-π and hydrogen bonding interaction. The synthesized MIP was more selective for *p*-CP due to the donating electron properties of chlorine substituents, which improved the electron-donor-acceptor interaction between adsorbent and adsorbate. Even though this MIP is selective to *p*-CP, it is also able to recognize any molecule similar to HQ.

Accepted

■ ACKNOWLEDGMENTS

This research has been carried out under University Fundamental Research Grants (GPUF) (grant code: 2022-0123-101-01) provided by the Universiti Pendidikan Sultan Idris (UPSI), Malaysia. The authors would like to extend their gratitude to the Research, Management and Innovation Centre (RMIC), UPSI that manages the grants.

■ CONFLICT OF INTEREST

The authors have no conflict of interest

■ AUTHOR CONTRIBUTIONS

Norlin Suhaiza Musali, Norlaili Abu Bakar, and Nurulsaidah Abdul Rahim conducted the experiment, wrote, and revised the manuscript. Wan Rusmawati Wan Mahamod, Norhayati Hashim, Sharifah Norain Mohd Sharif, Siti Kamilah Che Soh, and Alizar Ulianas, revised the manuscript. All authors agreed to the final version of this manuscript.

■ REFERENCES

[1] Ahmad, K., Kumar, P., and Mobin, S.M., 2020, A highly sensitive and selective hydroquinone sensor based on a newly designed N-rGO/$SrZrO_3$ composite, *Nanoscale Adv.*, 2 (1), 502–511.

[2] Ma, X., Liu, Z., Qiu, C., Chen, T., and Ma, H., 2013, Simultaneous determination of hydroquinone and catechol based on glassy carbon electrode modified with gold-graphene nanocomposite, *Microchim. Acta*, 180 (5), 461–468.

[3] Enguita, F.J., and Leitão, A.L., 2013, Hydroquinone: Environmental pollution, toxicity, and microbial answers, *BioMed Res. Int.*, 2013 (1), 542168.

[4] Fabian, I.M., Sinnathamby, E.S., Flanagan, C.J., Lindberg, A., Tynes, B., Kelkar, R.A., Varrassi, G., Ahmadzadeh, S., Shekooh, S., and Kaye, A.D., 2023, Topical hydroquinone for hyperpigmentation: A narrative review monitoring, *Cureus*, 15 (11), e48840.

[5] Hammani, H., Laghrib, F., Farahi, A., Lahrich, S., El Ouafy, T., Aboulkas, A., El Harfi, K., and El Mhammedi, M.A., 2019, Preparation of activated carbon from date stones as a catalyst to the reactivity of hydroquinone: Application in skin whitening cosmetics samples, *J. Sci.: Adv. Mater. Devices*, 4 (3), 451–458.

[6] Santos, A., Yustos, P., Quintanilla, A., García-Ochoa, F., Casas, J.A., and Rodriguez, J.J., 2004, Evolution of toxicity upon wet catalytic oxidation of phenol, *Environ. Sci. Technol.*, 38 (1), 133–138.

[7] Owolabi, J.O., Fabiyi, O.S., Adelakin, L.A., and Ekwerike, M.C., 2020, Effects of skin lightening cream agents - Hydroquinone and kojic acid, on the skin of adult female experimental rats, *Clin., Cosmet. Invest. Dermatol.*, 13, 283–289.

[8] Chen, X., Wei, X., Wang, J., Yang, Y., Wang, Y., Li, Q., and Wang, S., 2020, Toxicity removal and biodegradability enhancement of sludge extract in hydroquinone-rich wastewater via cultivation of *Chlorella vulgaris*, *J. Cleaner Prod.*, 277, 124030.

[9] Ibrahim, F., Sharaf El-Din, M.K., El-Deen, A.K., and Shimizu, K., 2019, A new HPLC-DAD method for the concurrent determination of hydroquinone, hydrocortisone acetate and tretinoin in different pharmaceuticals for melasma treatment, *J. Chromatogr. Sci.*, 57 (6), 495–501.

[10] Moldovan, Z., Popa, D.E., David, I.G., Buleandra, M., and Badea, I.A., 2017, A derivative spectrometric method for hydroquinone determination in the presence of kojic acid, glycolic acid, and ascorbic acid, *J. Spectrosc.*, 2017 (1), 6929520.

[11] Amola, L.A., Kamgaing, T., Tiegam Tagne, R.F., Atemkeng, C.D., Kuete, I.H.T., and Anagho, S.G., 2022, Optimized removal of hydroquinone and resorcinol by activated carbon based on shea residue (*Vitellaria paradoxa*): Thermodynamics, adsorption mechanism, nonlinear kinetics, and isotherms, *J. Chem.*, 2022 (1), 1125877.

[12] Shengli, S., Junping, L., Qi, L., Fangru, N., Jia, F., and Shulian, X., 2018, Optimized preparation of *Phragmites australis* activated carbon using the Box-Behnken method and desirability function to remove hydroquinone, *Ecotoxicol. Environ. Saf.*, 165, 411–422.

Accepted

[13] Peng, Y., Tang, Z., Dong, Y., Che, G., and Xin, Z., 2018, Electrochemical detection of hydroquinone based on MoS_2/reduced graphene oxide nanocomposites, *J. Electroanal. Chem.*, 816, 38–44.

[14] Sun, X., Xie, Y., Chu, H., Long, M., Zhang, M., Wang, Y., and Hu, X., 2022, A highly sensitive electrochemical biosensor for the detection of hydroquinone based on a magnetic covalent organic framework and enzyme for signal amplification, *New J. Chem*., 46 (24), 11902–11909.

[15] Karthika, A., Ramasamy Raja, V., Karuppasamy, P., Suganthi, A., and Rajarajan, M., 2020, A novel electrochemical sensor for determination of hydroquinone in water using $FeWO_4/SnO_2$ nanocomposite immobilized modified glassy carbon electrode, *Arabian J. Chem.*, 13 (2), 4065–4081.

[16] Wang, Y., Liu, Y., and Yang, M., 2020, Molecularly imprinted electrochemiluminescence sensor for sensitive and selective detection of hydroquinone molecularly imprinted electrochemiluminescence sensor for sensitive and selective detection of hydroquinone, *Chem. Lett*., 49 (7), 855–858.

[17] Shafqat, S.R., Bhawani, S.A., Bakhtiar, S., and Ibrahim, M.N.M., 2020, Synthesis of molecularly imprinted polymer for removal of Congo red, *BMC Chem.*, 14 (1), 27.

[18] Malik, M.I., Shaikh, H., Mustafa, G., and Bhanger, M.I., 2019, Recent applications of molecularly imprinted polymers in analytical chemistry, *Sep. Purif. Rev.*, 48 (3), 179–219.

[19] Bates, F., Busato, M., Piletska, E., Whitcombe, M.J., Karim, K., Guerreiro, A., del Valle, M., Giorgetti, A., and Piletsky, S., 2017, Computational design of molecularly imprinted polymer for direct detection of melamine in milk, *Sep. Sci. Technol*., 52 (8), 1441–1453.

[20] Cheong, W.J., Yang, S.H., and Ali, F., 2013, Molecular imprinted polymers for separation science: A review of reviews, *J. Sep. Sci*., 36 (3), 609–628.

[21] Sajini, T., Gigimol, M.G., and Mathew, B., 2019, A brief overview of molecularly Imprinted polymers supported on titanium dioxide matrices, *Mater. Today Chem*., 11, 283–295.

[22] Cui, Y., He, Z., Xu, Y., Su, Y., Ding, L., and Li, Y., 2020, Fabrication of molecularly imprinted polymers with tunable adsorption capability based on solvent-responsive, *Chem. Eng. J*., 405, 126608.

[23] Poole, C.F., Poole, S.K., 2012, "Principles and Practice of Solid-Phase Extraction" in *Comprehensive Sampling and Sample Preparation*, Eds. Pawliszyn, J., Academic Press, Oxford, UK, 273–297.

[24] Shen, Y., Miao, P., Liu, S., Gao, J., Han, X., Zhao, Y., and Chen, T., 2023, Preparation and application progress of imprinted polymers, *Polymers*, 15 (10), 2344.

[25] Pupin, R.R., Foguel, M.V., Gonçalves, L.M., and Sotomayor, M.P.T., 2020, Magnetic molecularly imprinted polymers obtained by photopolymerization for selective recognition of penicillin G, *J. Appl. Polym. Sci.*, 137 (13), 48496.

[26] Kan, X., Zhao, Q., Zhang, Z., Wang, Z., and Zhu, J.J., 2008, Molecularly imprinted polymers microsphere prepared by precipitation polymerization for hydroquinone recognition, *Talanta*, 75 (1), 22–26.

[27] Singh, R., and Singh, M., 2022, Highly selective and specific monitoring of pollutants using dual template imprinted MIP sensor, *J. Electroanal. Chem.*, 926, 116939.

[28] Shafqat, S.R., Bhawani, S.A., Bakhtiar, S., Ibrahim, M.N.M., and Shafqat, S.S., 2023, Template-assisted synthesis of molecularly imprinted polymers for the removal of methyl red from aqueous media, *BMC Chem.*, 17 (1), 46.

[29] Yu, H., He, Y., She, Y., Wang, M., Yan, Z., Ren, J.H., Cao, Z., Shao, Y., Wang, S., Abd El-Aty, A.M., Hacımüftüoğlu, A., and Wang, J., 2019, Preparation of molecularly imprinted polymers coupled with high-performance liquid chromatography for the selective extraction of salidroside from *Rhodiola crenulata*, *J. Chromatogr. B: Anal. Technol. Biomed. Life Sci.*, 1118-1119, 180–186.

[30] Hasanah, A.N., Susanti, I., Marcellino, M., Maranata, G.J., Saputri, F.A., and Pratiwi, R., 2021, Microsphere molecularly imprinted solid-phase extraction for diazepam analysis using itaconic acid

Accepted

as a monomer in propanol, *Open Chem*., 19 (1), 604–613.

[31] Edet, U.A., and Ifelebuegu, A.O., 2020, Kinetics, isotherms, and thermodynamic modeling of the adsorption of phosphates from model wastewater using recycled brick waste, *Process*, 8 (6), 665.

[32] Langmuir, I., 1918, The adsorption of gases on plane surfaces of glass, mica and platinum, *J. Am. Chem. Soc.*, 40 (9), 1361–1403.

[33] Szczepaniak, W., Zabłocka-Malicka, M., Pasiecznik, I., Pohl, P., and Rutkowski, P., 2018, Adsorption of La^{3+} and Dy^{3+} ions on biohydroxyapatite obtained from pork bones gasified with steam, *Environ. Prot. Eng.*, 44 (1), 29–40.

[34] Pizan-aquino, C., Wong, A., Avilés-Félix, L., Khan, S., Picasso, G., and Sotomayor, M.D.P.T., 2020, Evaluation of the performance of selective M-MIP to tetracycline using electrochemical and HPLC-UV method, *Mater. Chem. Phys*., 245, 122777.

[35] Desta, M.B., 2013, Batch sorption experiments: Langmuir and Freundlich isotherm studies for the adsorption of textile metal ions onto teff straw (*Eragrostis tef*) agricultural waste, *J. Thermodyn*., 2013 (1), 375830.

[36] Sun, M., Li, Y., Sha, S., Gao, J., Wang, R., Zhang, Y., Hao, Q., Chen, H., Yao, Q., and Ma, X., 2020, The composition and structure of *n*-hexane insoluble-hot benzene soluble fraction and hot benzene insoluble fraction from low temperature coal tar, *Fuel*, 262, 116511.

[37] Liu, Y., Wang, Q., Guo, S., Jia, P., Shui, Y., Yao, S., Huang, C., Zhang, M., and Wang, L., 2018, Highly selective and sensitive fluorescence detection of hydroquinone using novel silicon quantum dots, *Sens. Actuators, B*, 275, 415–421.

[38] Sharma, G., and Kandasubramanian, B., 2020, Molecularly imprinted polymers for selective recognition and extraction of heavy metal ions and toxic dyes, *J. Chem. Eng. Data*, 65 (2), 396–418.

[39] Shim, D.Y., Chang, S.M., and Kim, J.M., 2021, Development of fast resettable gravimetric aromatic gas sensors using quartz crystal microbalance, *Sens. Actuators, B*, 329, 129143.

[40] Tolkou, A.K., Kyzas, G.Z., and Katsoyiannis, I.A., 2022, Arsenic(III) and Arsenic(V) removal from water sources by molecularly imprinted polymers (MIPs): A mini review of recent developments, *Sustainability*, 14 (9), 5222.

[41] Limthin, D., Klamchuen, A., and Phromyothin, D., 2019, Surface modification of superparamagnetic iron oxide nanoparticles and methyl methacrylate molecularly imprinted polymer for gluten detection, *Ferroelectrics*, 552 (1), 97–107.

[42] Bakhtiar, S., Bhawani, S.A., and Shafqat, S.R., 2019, Synthesis and characterization of molecular imprinting polymer for the removal of 2-phenylphenol from spiked blood serum and river water, *Chem. Biol. Technol. Agric.*, 6 (1), 15.

[43] Retnaningtyas, Y., Supriyanto, G., Tri Puspaningsih, N.N., Irawan, R., and Siswodihardjo, S., 2021, A novel molecular imprinting polymer for the selective adsorption of D-arabinitol from spiked urine, *Turk. J. Chem*., 44 (6), 1265–1277.

[44] Guo, P., Yang, W., Hu, H., Wang, Y., and Li, P., 2019, Rapid detection of aflatoxin B1 by dummy template molecularly imprinted polymer capped CdTe quantum dots, *Anal. Bioanal. Chem*., 411 (12), 2607–2617.

[45] Masumoto, S., Nakamura, Y., and Haginaka, J., 2021, Molecularly imprinted polymers for arbutin and rutin by modified precipitation polymerization and their application for selective extraction of rutin in nutritional supplements, *J. Pharm. Biomed. Anal.*, 205, 114294.

[46] Comeau, P.A., and Willett, T.L., 2020, Triethyleneglycol dimethacrylate addition improves the 3D-printability and construct properties of a GelMA-nHA composite system towards tissue engineering applications, *Mater. Sci. Eng., C*, 112, 110937.

[47] Rubahamya, B., Kumar Reddy, K.S., Prabhu, A., Al Shoaibi, A., and Srinivasakannan, C., 2019, Porous carbon screening for benzene sorption, *Environ. Prog. Sustain. Energy*, 38 (S1), 93–99.

[48] Grissom, T.G., Sharp, C.H., Usov, P.M., Troya, D., Morris, A.J., and Morris, J.R., 2018, Benzene,

Accepted

toluene, and xylene transport through UiO-66: Diffusion rates, energetics, and the role of hydrogen bonding, *J. Phys. Chem. C*, 122 (28), 16060–16069.

[49] Mohanadas, D., Tukimin, N., and Sulaiman, Y., 2019, Simultaneous electrochemical detection of hydroquinone and catechol using poly(3,4-ethylenedioxythiophene)/reduced graphene oxide/manganese dioxide, *Synth. Met*., 252, 76–81.

[50] Loreto, S., Cuypers, B., Brokken, J., Van Doorslaer, S., De Wael, K., and Meynen, V., 2017, The effect of the buffer solution on the adsorption and stability of horse heart myoglobin on commercial mesoporous titanium dioxide: A matter of the right choice, *Phys. Chem. Chem. Phys*., 19, 13503.

[51] Cantarella, M., Carroccio, S.C., Dattilo, S., Avolio, R., Castaldo, R., Puglisi, C., and Privitera, V., 2019, Molecularly imprinted polymer for selective adsorption of diclofenac from contaminated water, *Chem. Eng. J*., 367, 180–188.

[52] Anirudhan, T.S., and Anju, S.M., 2019, Synthesis and evaluation of TiO_2 nanotubes/silylated graphene oxide-based molecularly imprinted polymer for the selective adsorption and subsequent photocatalytic degradation of 2,4-dichlorophenoxyacetic, *J. Environ. Chem. Eng.*, 7 (5), 103355.

[53] Amatatongchai, M., Sitanurak, J., Sroysee, W., Sodanat, S., Chairam, S., Jarujamrus, P., Nacapricha, D., and Lieberzeit, P.A., 2019, Highly sensitive and selective electrochemical paper-based device using a graphite screen-printed electrode modified with molecularly imprinted polymers coated Fe_3O_4@Au@SiO_2 for serotonin determination, *Anal. Chim. Acta*, 1077, 255–265.

[54] Wang, X., Wang, M., Wu, B., Yu, S., Liu, Z., Qin, X., Xu, H., Li, W., Luo, S., Wang, L., Ma, C., and Liu, S., 2024, Magnetic molecularly imprinted polymers using ternary deep eutectic solvent as novel functional monomer for hydroxytyrosol separation, *Heliyon*, 10 (8), e28257.

[55] Hanbali, G., Jodeh, S., Hamed, O., Bol, R., Khalaf, B., Qdemat, A., Samhan, S., and Dagdag, O., 2020, Magnetic multiwall carbon nanotube decorated with novel functionalities: Synthesis and application as adsorbents for lead removal from aqueous medium, *Processes*, 8 (8), 986.

[56] Khoo, W.C., Kamaruzaman, S., Lim, H.N., Md. Jamil, S.N.A., and Yahaya, N., 2019, Synthesis and characterization of graphene oxide-molecularly imprinted polymer for Neopterin adsorption study, *J Polym Res*., 26 (8), 184.

[57] Bagheri, A.R., Aramesh, N., Khan, A.A., Gul, I., Ghotekar, S., and Bilal, M., 2021, Molecularly imprinted polymers-based adsorption and photocatalytic approaches for mitigation of environmentally-hazardous pollutants - A review, *J. Environ. Chem. Eng.*, 9 (1), 104879.

[58] Rajadhiraj, R., and Nandiyanto, A.B.D., 2022, Curcumin adsorption on zinc imidazole framework-8 particles: Isotherm adsorption using Langmuir, Freundlich, Temkin, and Dubinin-Radushkevich models, *J. Eng. Sci. Technol*., 17 (2), 1078–1089.

[59] Hou, L., Han, X., and Wang, N., 2020, High performance of molecularly imprinted polymer for the selective adsorption of erythromycin in water, *Colloid. Polym. Sci.*, 298 (8), 1023–1033.

[60] Li, Y., Wang, Y., Wang, M., Zhang, J., Wang, Q., and Li, H., 2020, A molecularly imprinted nanoprobe incorporating Cu_2O@Ag nanoparticles with different morphologies for selective SERS based detection of chlorophenols, *Microchim. Acta*, 187 (1), 59.

[61] Zhang, Z., Sun, D., Li, G., Zhang, B., Zhang, B., Qiu, S., Li, Y., and Wu, T., 2019, Calcined products of Mg–Al layered double hydroxides/single-walled carbon nanotubes nanocomposites for expeditious removal of phenol and 4-chlorophenol from aqueous solutions, *Colloids Surf., A*, 565, 143–153.

Accepted